



OPEN Structural changes in vortex vein ampullae in eyes with pachychoroid-spectrum disorder

Ryoh Funatsu¹, Hiroto Terasaki¹✉, Shozo Sonoda¹, Naohisa Mihara¹, Mariko Hirokawa², Yasushi Tanabe², Hideki Shiihara¹ & Taiji Sakamoto¹

The purpose of this study is to identify the characteristics of vortex vein ampullae in pachychoroid-spectrum disorders. This case-control study evaluated vortex vein ampullae using Optos Silverstone, an imaging device combining ultra-widefield scanning laser fundus imaging with swept-source optical coherence tomography. Consecutive patients with pachychoroid-spectrum disorders and controls who visited Kagoshima university hospital between January 2022 and December 2023 and underwent vortex vein ampullae evaluations. We compared morphological parameters of supratemporal and infratemporal vortex vein ampullae between eyes with pachychoroid-spectrum disorders and control subjects. We included 40 patients (46 eyes) with pachychoroid-spectrum disorders, and 14 healthy controls (15 eyes). We observed no significant differences in any supratemporal vortex vein ampullae morphological parameters ($P \geq 0.487$ for all comparisons). In infratemporal vortex vein ampullae, eyes with pachychoroid-spectrum disorders showed significantly larger mean luminal volume ($6.9 \times 10^6 \pm 1.8 \times 10^6$ pixels vs. $4.7 \times 10^6 \pm 1.5 \times 10^6$ pixels, $P < 0.001$) and greater mean vessel diameter ($P = 0.040$) compared to controls, with no significant differences in luminal proportions ($P = 0.353$). After adjusting for potential confounders, the pachychoroid-spectrum disorders group still demonstrated significantly larger infratemporal vortex vein ampullae luminal volume and mean vessel diameter compared to controls ($P \leq 0.011$ for both analyses). Enlargement of lumen and stroma was observed exclusively in the infratemporal vortex vein ampullae in eyes with pachychoroid-spectrum disorders. Impaired choroidal drainage alone may not fully account for the observed vortex vein ampullae alterations.

Pachychoroid spectrum disorders (PSDs) represent a phenotype of age-related macular degeneration (AMD), the leading cause of irreversible vision loss in industrialized nations^{1–7}. PSD responds differently to anti-vascular endothelial growth factor therapies and photodynamic therapy than does conventional AMD, suggesting its distinct pathogenesis^{5,7–9}. Elucidating PSD pathogenesis is critical for facilitating the development of personalized management strategies for AMD.

A pathogenetic hypothesis termed “venous overload choroidopathy” has been proposed to explain one potential cause of PSD^{10–14}. This hypothesis suggests that scleral thickening increases outflow resistance in the vortex veins, consequently inducing stasis in the choroidal venous system. Despite advances in widefield choroidal imaging, current techniques have limitations. Ultrawidefield indocyanine green angiography lacks three-dimensional visualization capabilities^{15–17}, whereas widefield optical coherence tomography (OCT) can only visualize the vicinity of the vortex vein ampullae (VVA)^{13,14,18}. These technological constraints have hindered the development of a standardized method for comprehensive VVA structure assessment. Consequently, the morphological characteristics of the VVA in eyes with PSD remain largely unknown, despite their crucial role in PSD pathogenesis^{19–24}. Optos Silverstone (Optos, UK) has recently emerged as an innovative imaging system that integrates ultrawidefield scanning laser fundus imaging (200° field of view)-guided swept-source OCT²⁵. The expanded field of view of this device enables OCT imaging of the fundus periphery, where the VVA are located, from a frontal perspective. Such advancements have revealed potential pathogenic mechanisms in various retinal and choroidal diseases^{18–20}.

This study aims to elucidate the VVA characteristics in PSD by developing an evaluation method for the three-dimensional structure of VVA using Optos Silverstone.

¹Department of Ophthalmology, Kagoshima University Graduate School of Medical and Dental Sciences, 8-35-1, Sakuragaoka, Kagoshima, Kagoshima, Japan. ²Healthcare Business Unit, Nikon Corporation, Tokyo, Japan. ✉email: teracchi@m2.kufm.kagoshima-u.ac.jp

Characteristics	PSD N = 46	Healthy N = 15	P value
Mean age \pm SD; median, years	56.2 \pm 11.6; 53.0	62.3 \pm 15.9; 66.0	0.090
Female, n (%)	12 (26.1)	7 (46.7)	0.199
The type of PSD, n (%)			
CSC	32 (69.6)	–	
PPE	9 (19.6)	–	
PNV	4 (8.7)	–	
PCV	1 (2.2)	–	
Mean axial length \pm SD; median, mm	23.7 \pm 1.2; 23.9	23.2 \pm 1.4; 23.4	0.113
Mean CCT \pm SD; median, μ m	390.9 \pm 117.5; 360.0	304.3 \pm 90.0; 315.0	0.015
Running patterns of Haller vessel, n (%)			
Symmetry	13 (28.3)	11 (73.3)	0.010
Upper dominant	23 (50.0)	3 (20.0)	
Lower dominant	10 (21.7)	1 (6.7)	

Table 1. Comparisons of patient characteristics between PSD and healthy participants. P-values were calculated using the Mann-Whitney U test for continuous variables and Fisher's exact test for qualitative variables. PSD pachychoroid-spectrum disorders, SD standard deviation, CSC central serous chorioretinopathy, PPE pachychoroid pigment epitheliopathy, PNV pachychoroid neovascularopathy, PCV polypoidal choroidal vascularopathy, CCT central choroidal thickness.

Characteristics	PSD, N = 46	Healthy, N = 15	P value
Supratemporal			
Mean luminal volume \pm SD; median, pixels	6.8*10 ⁶ \pm 2.4*10 ⁶ ; 7.1*10 ⁶	6.5*10 ⁶ \pm 2.7*10 ⁶ ; 6.4*10 ⁶	0.693
Mean luminal proportion \pm SD; median	0.28 \pm 0.05; 0.28	0.29 \pm 0.05; 0.29	0.839
Mean length \pm SD; median, pixels	4.2*10 ³ \pm 1.0*10 ³ ; 4.2*10 ³	4.3*10 ³ \pm 1.1*10 ³ ; 4.3*10 ³	0.863
Mean diameter \pm SD; median, pixels	22.6 \pm 3.8; 23.0	21.6 \pm 2.9; 22.1	0.487
Infratemporal			
Mean luminal volume \pm SD; median, pixels	6.9*10 ⁶ \pm 1.8*10 ⁶ ; 6.9*10 ⁶	4.7*10 ⁶ \pm 1.5*10 ⁶ ; 4.4*10 ⁶	< 0.001
Mean luminal proportion \pm SD; median	0.30 \pm 0.04; 0.30	0.29 \pm 0.04; 0.28	0.353
Mean length \pm SD; median, pixels	4.0*10 ³ \pm 1.0*10 ³ ; 4.1*10 ³	3.2*10 ³ \pm 8.5*10 ² ; 3.2*10 ³	0.021
Mean diameter \pm SD; median, pixels	23.7 \pm 2.8; 23.7	21.8 \pm 2.2; 22.2	0.040

Table 2. Comparisons of vortex vein ampullae morphological parameters between PSD and healthy participants. P-values were calculated using the Mann-Whitney U test. PSD pachychoroid-spectrum disorders, SD standard deviation.

Results

Patient characteristics

We included 40 patients (46 eyes) with PSD (CSC, 32 eyes [69.6%]; PPE, 9 eyes [19.6%]; PNV, 4 eyes [8.7%]; PCV, 1 eye [2.2%]) and 14 healthy controls (15 eyes). Table 1 shows the detailed patient characteristics. Compared with the healthy group, the PSD group demonstrated significantly greater CCT ($P=0.015$) and a lower proportion of symmetrical Haller vessel running patterns ($P=0.010$). In the PSD group vs. the healthy group, the patterns were distributed as follows: upper dominant (50.0% vs. 20.0%), lower dominant (21.7% vs. 6.7%), and symmetrical (28.3% vs. 73.3%).

Comparisons of VVA morphology between PSD eyes and healthy eyes

We observed no significant differences in the supratemporal VVA morphological parameters between PSD eyes and healthy eyes ($P \geq 0.487$ for all comparisons, Table 2 and Fig. S1). For infratemporal VVA, eyes with PSD presented a significantly greater mean luminal volume (PSD vs. healthy, $6.9 \times 10^6 \pm 1.8 \times 10^6$ pixels vs. $4.7 \times 10^6 \pm 1.5 \times 10^6$ pixels, $P < 0.001$). The mean vessel diameter and total vessel length of infratemporal VVA in the PSD were significantly greater in the PSD group than in the control group ($P \leq 0.021$ for both comparisons). In contrast, no significant difference in the vessel luminal proportion in the infratemporal VVA region was detected between the groups ($P=0.353$).

After adjusting for potential confounders, the PSD group demonstrated significantly greater infratemporal VVA luminal volume and vessel diameter than the healthy group did ($P \leq 0.011$ for both comparisons, Table S1). However, no clear difference was observed in the total vessel length ($P=0.220$). Comparison of VVA morphology among PSD subtypes (excluding PCV) revealed no significant differences (Table S2).

Comparisons of VVA morphology among running patterns of the Haller vessel for eyes with PSD

The upper dominant group exhibited the largest supratemporal VVA volume ($P=0.040$, Table 3), whereas the lower dominant group presented the largest infratemporal VVA volume ($P=0.111$). Compared with the lower dominant group, the upper dominant group presented significantly greater vertical differences in luminal volume (Steel-Dwass test: upper dominant vs. lower dominant, $P=0.006$; symmetry vs. upper dominant, $P=0.476$; symmetry vs. lower dominant, $P=0.139$).

The vertical differences in the luminal proportion and mean vessel diameter demonstrated a similar trend as that for the luminal volume (Steel-Dwass test: luminal proportion, upper dominant vs. lower dominant, $P=0.003$; mean vessel diameter, upper dominant vs. lower dominant, $P=0.001$). Figure 1 illustrates a representative case with VVA evaluations. Similar to the PSD group, healthy subjects with upper dominance showed greater supratemporal VVA volume (Table S3).

Associations between VVA morphology and patient characteristics

The infratemporal VVA luminal volume was significantly positively associated with CCT ($\beta=0.7 \times 10^4$, $P=0.004$) and negatively associated with age ($\beta=-6.1 \times 10^4$, $P=0.005$) but was not significantly associated with axial length or sex ($P \geq 0.101$ for both analyses, Fig. 2 and Table S4). The infratemporal VVA mean vessel diameter was significantly positively associated with CCT ($P=0.011$) and negatively associated with axial length ($P=0.014$) but was not significantly associated with age or sex ($P \geq 0.698$ for both analyses). No patient characteristics were significantly associated with the supratemporal VVA luminal volume or mean vessel diameter ($P \geq 0.099$ for all analyses). Sex was not significantly associated with any of the VVA morphological parameters ($P \geq 0.088$ for all analyses).

Discussion

This study quantitatively assessed VVA morphology in PSD patients via a developed evaluation technique. Compared with healthy eyes, PSD eyes presented significantly greater vessel luminal volume and mean vessel diameter and no significant differences in supratemporal VVA morphology. Moreover, eyes with PSD presented an enlarged VVA lumina on the dominant side of the macular Haller vessels.

Advances in OCT technology, including faster scan speeds and enhanced depth imaging, have revealed characteristic features of PSD eyes: choroidal thickening, increased choroidal lumen fraction, enlarged vascular diameter, fluid loculation, and asymmetry of the macular Haller's vessels in the posterior pole^{3,26–29}. Furthermore, most studies using widefield OCT have demonstrated choroidal thickening and an enlarged vascular diameter extending to the midperiphery in PSD eyes^{13,14,30}. However, Maruko et al., utilizing OCT with the widest field of view, reported minimal differences in peripheral choroidal thickness between PSD eyes and normal eyes³¹. These findings suggest that venous choroidal overload and interstitial fluid retention extend from the macula toward the VVA, potentially diminishing in the peripheral VVA region^{13,14,30,31}. In eyes with PSD, our study revealed an enlargement of both the lumen and stroma only in the inferior VVA, whereas the superior VVA remained

Characteristics	Symmetry N = 13	Upper dominant N = 23	Lower dominant N = 10	P value
Mean luminal volume \pm SD; median, pixels				
Supratemporal	7.0*10 ⁶ \pm 3.4*10 ⁶ ; 6.7*10 ⁶	7.4*10 ⁶ \pm 1.9*10 ⁶ ; 7.6*10 ⁶	5.5*10 ⁶ \pm 1.7*10 ⁶ ; 5.5*10 ⁶	0.040
Infratemporal	6.5*10 ⁶ \pm 1.8*10 ⁶ ; 6.0*10 ⁶	6.7*10 ⁶ \pm 2.0*10 ⁶ ; 6.9*10 ⁶	7.9*10 ⁶ \pm 1.3*10 ⁶ ; 8.2*10 ⁶	0.111
Vertical difference	0.7*10 ⁶ \pm 4.1*10 ⁶ ; 0.5*10 ⁶	1.5*10 ⁶ \pm 2.3*10 ⁶ ; 1.8*10 ⁶	- 2.4*10 ⁶ \pm 2.4*10 ⁶ ; - 3.3*10 ⁶	0.007
Total: superior + inferior	13.3*10 ⁶ \pm 4.0*10 ⁶ ; 12.2*10 ⁶	13.9*10 ⁶ \pm 2.6*10 ⁶ ; 14.5*10 ⁶	13.3*10 ⁶ \pm 2.0*10 ⁶ ; 13.8*10 ⁶	0.479
Luminal proportion				
Supratemporal	0.28 \pm 0.06; 0.29	0.30 \pm 0.04; 0.31	0.24 \pm 0.04; 0.25	0.008
Infratemporal	0.29 \pm 0.04; 0.30	0.30 \pm 0.04; 0.30	0.31 \pm 0.05; 0.31	0.680
Vertical difference	- 0.02 \pm 0.07; - 0.04	0.01 \pm 0.05; 0.02	- 0.07 \pm 0.05; - 0.06	0.006
Mean length \pm SD; median, pixels				
Supratemporal	4.2*10 ³ \pm 0.8*10 ³ ; 4.0*10 ³	4.4*10 ³ \pm 0.8*10 ³ ; 4.4*10 ³	4.1*10 ³ \pm 1.5*10 ³ ; 3.2*10 ³	0.392
Infratemporal	3.8*10 ³ \pm 1.1*10 ³ ; 3.9*10 ³	4.0*10 ³ \pm 1.0*10 ³ ; 4.0*10 ³	4.1*10 ³ \pm 0.9*10 ³	0.796
Vertical difference	551.1 \pm 1,033.6; 901.0	545.3 \pm 1,105.0; 464.0	56.9 \pm 1,685.3; - 107.0	0.697
Total: superior + inferior	7.8*10 ³ \pm 1.7*10 ³ ; 8.3*10 ³	8.2*10 ³ \pm 1,529.240; 8.2*10 ³	8.3*10 ³ \pm 2.0*10 ³ ; 7.7*10 ³	0.871
Mean diameter \pm SD; median, pixels				
Supratemporal	23.0 \pm 5.9; 21.6	23.3 \pm 2.6; 23.9	21.0 \pm 2.7; 20.4	0.064
Infratemporal	23.7 \pm 3.0; 24.3	23.0 \pm 2.5; 23.0	25.0 \pm 3.2; 23.7	0.408
Vertical difference	- 1.0 \pm 4.6; - 0.9	0.8 \pm 2.2; 1.4	- 4.4 \pm 3.1; - 5.0	0.003
Total: superior + inferior	46.9 \pm 8.8; 44.2	46.4 \pm 4.3; 46.0	45.5 \pm 4.9; 44.9	0.708

Table 3. Comparisons of vortex vein ampullae morphological parameters among the running patterns of Haller's vessel for eyes with PSD. P-values were calculated using the Kruskal-Wallis test. PSD pachychoroid-spectrum disorders, SD standard deviation.

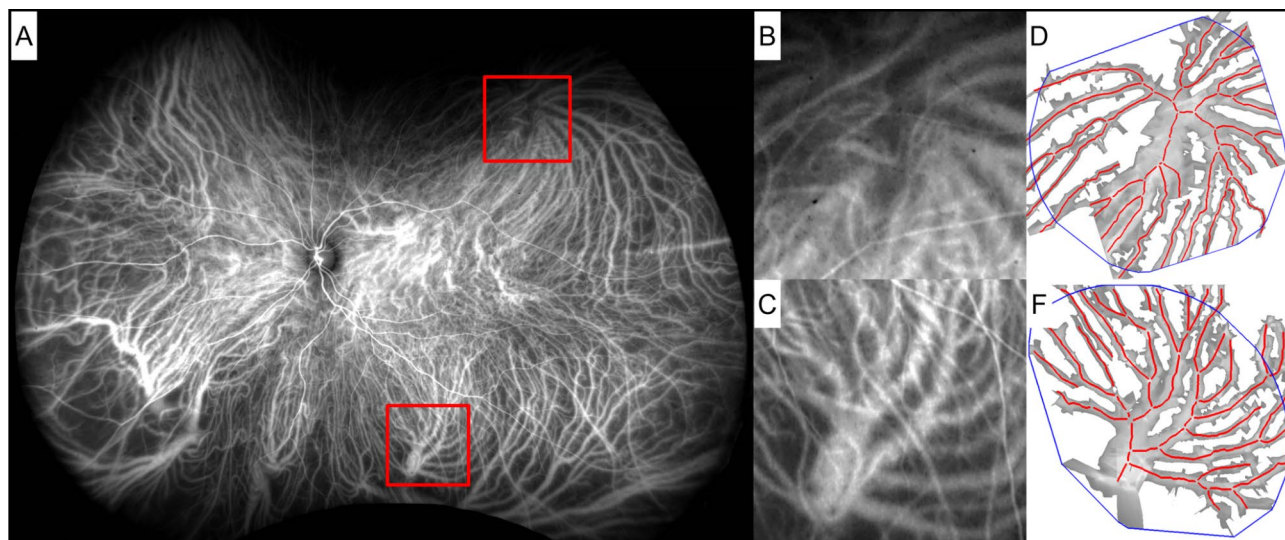


Fig. 1. Vortex vein ampullae images of a patient with the upper-dominant Haller vessel pattern. **(A)** This ICGA image shows a 55-year-old male patient with CSC. The axial length was 24.3 mm, and the Haller vessel running pattern was the upper-dominant type. **(B,C)** Enlarged views of the supratemporal and infratemporal VVA in the ICGA image. **(D,E)** Three-dimensional structures of the VVA acquired via ultrawidefield scanning laser fundus image-guided swept-source OCT. The luminal volume was 7,578,810 pixels for the supratemporal VVA and 4,705,821 pixels for the infratemporal VVA. CSC central serous chorioretinopathy, ICGA indocyanine green angiography, VVA vortex vein ampulla, OCT optical coherence tomography.

comparable to that of control eyes. If a scleral thickening-induced increase in choroidal outflow resistance could fully explain PSD changes^{10,11,26}, entire choroidal expansion from the VVA to the macula may potentially be observed. We cannot exclude the possibility that scleral properties limited changes in VVA morphology. However, since the sclera blocks OCT laser penetration, we think that intrascleral choroidal vessels are largely excluded from our analysis. Therefore, these findings indicate that impaired choroidal blood drainage alone cannot fully account for the pathogenesis of PSD.

Saito et al. proposed choroidal hyperperfusion as a key feature in the active phase of acute CSC³². Short posterior ciliary arteries, the choroid's primary inflow vessels, are distributed in the posterior pole and are concentrated around the macula^{33,34}. Choroidal hyperperfusion increases macular choroidal blood flow, elevates venous pressure and causes vascular dilation, while it may promote interstitial fluid accumulation. The selective enlargement of the lumen and interstitium in the inferior VVA region, which is absent in the superior VVA, might indicate gravitational accumulation of excessive macular fluid.

Choroidal morphology and perfusion in PSD are reportedly regionally imbalanced^{28,29,35}. Using widefield OCT, Ishikura et al. reported that eyes with asymmetrically enlarged macular choroidal vessels also exhibited choroidal thickening near the VVA on the dominant side¹³. Our study demonstrated VVA enlargement on the dominant side, indicating that asymmetric vascular dilation extends beyond the macula to include the VVA. However, the etiology of this choroidal asymmetry remains elusive.

Takahashi et al. demonstrated an imbalance in perfusion zones and vortex vein systems via postscleral buckling ICGA³⁶. Additionally, Matsumoto et al. reported predominant asymmetric choroidal vessel expansion on the ligated side in a monkey model following vortex vein occlusion³⁷. These findings indicate that choroidal venous outflow obstruction may induce asymmetry in the choroidal vasculature. However, several observations challenge the hypothesis that choroidal asymmetry results from acquired vascular pressure loading: (1) the resolution of asymmetric vessels approximately one month postvortex vein ligation in monkey models;³⁷ (2) a lack of an association between scleral thickness and choroidal vascular asymmetry;³⁸ (3) the presence of choroidal asymmetry in 40–50% of normal eyes;^{14,29,39,40} and (4) the absence of correlation between age and choroidal asymmetry⁴¹. Considering the absence of upper VVA dilation in our study, the effect of impaired choroidal drainage on macular choroidal asymmetry may be limited.

However, while Matsumoto et al. suggest that choroidal venous anastomoses may indicate venous outflow obstruction³⁷, these findings are also observed in normal eyes⁴⁰. In addition, there is the problem that the method of evaluating choroidal venous anastomoses is subjective. Quantitative assessment of choroidal venous anastomoses, rather than their mere presence, may help clarify their role in pachychoroid-spectrum disorders in future study.

There are several limitations to this study. First, because of its retrospective nature, future longitudinal studies are needed. Second, since the sample size of this study is relatively small, comparisons among PSD subtypes by larger surveys are warranted. Third, the lack of direct measurements of choroidal blood flow restricts the ability to elucidate the relationship between VVA morphological changes and hemodynamics. However, owing to the current lack of instruments capable of measuring peripheral choroidal blood flow, morphological evaluation serves as a necessary surrogate. To mitigate potential diurnal variations in macular choroidal thickness⁴², which

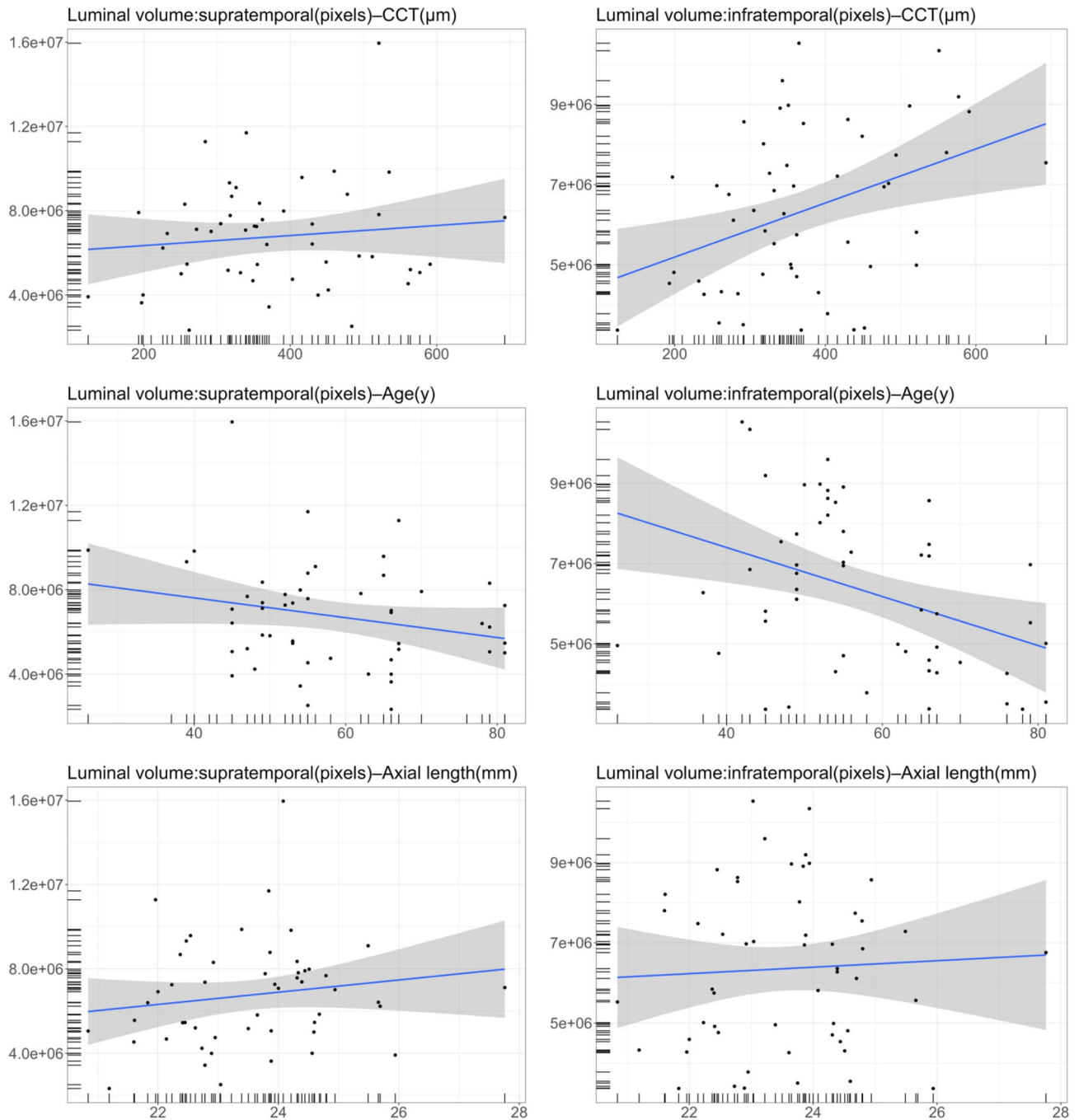


Fig. 2. Associations between the luminal volume of the VVA and patient characteristics. These scatter plots with regression lines and 95% confidence intervals illustrate the relationships between VVA parameters and patient characteristics. The luminal volume of the infratemporal VVA was positively associated with central choroidal thickness ($\beta = 0.7 \times 10^4$, $P = 0.004$) and negatively associated with age ($\beta = -6.1 \times 10^4$, $P = 0.005$). The associations between the luminal volume of supratemporal VVA and patient characteristics were not statistically significant ($P \leq 0.099$). VVA vortex vein ampulla, S supratemporal, I infratemporal.

may extend to VVA, examinations were confined to 8:30 am–12:30 pm. The pixel-to-micrometer ratio for each image is undetermined, potentially complicating comparisons between the quantitative values in this study and those derived from alternative methods. Further research is needed to elucidate the relationship between choroidal venous anastomoses and venous outflow obstruction.

In conclusion, enlargement of both the lumen and stroma was observed exclusively in the infratemporal VVA in eyes with PSD. Furthermore, asymmetry in macular choroidal morphology was observed to extend continuously to the VVA. While VVA morphology is implicated in PSD pathogenesis, impaired choroidal drainage alone may not fully account for the observed VVA alterations.

Methods

This was a single-center case-control study. This study was conducted as a retrospective observational study. Although informed consent was waived, an opt-out opportunity was provided to patients through the hospital bulletin board and website (The Ethics Committee of Kagoshima University, Kagoshima, Japan). The Ethics Committee approved this study (No. 16012), and all procedures were conducted in accordance with the tenets of the Declaration of Helsinki.

Patients

Consecutive patients with PSD who visited Kagoshima University Hospital between January 2022 and December 2023 and underwent VVA evaluation by Optos Silverstone were included. We also included a healthy group consisting of participants who underwent evaluation of the VVA in the same month as the PSD patients. These control patients were diagnosed with only cataracts and had no intraocular, optic nerve, infectious, or neoplastic diseases. On the basis of previous reports, PSD was defined by the following criteria: (1) the presence of dilated Haller vessels on OCT or indocyanine green angiography (ICGA), (2) choroidal vascular hyperpermeability on ICGA, and (3) the absence of soft drusen in the macular region^{3,6,20,21}. Among eyes fulfilling these PSD characteristics, we classified eyes as follows: pachychoroid neovascularopathy (PNV) for those with macular neovascularization (MNV) without polypoid lesions; pachychoroid polypoidal choroidal vasculopathy (PCV) when MNV was accompanied by polypoid lesions; central serous chorioretinopathy (CSC) in cases of serous retinal detachment without MNV; and pachychoroid pigment epitheliopathy (PPE) when only pigment epithelial detachment (PED) was present^{4,20,43–45}. Diagnoses were made by two retina specialists (RF, NM) in consultation, with any disagreements resolved by a senior supervisor (HT).

Data collection

We conducted comprehensive ophthalmic examinations and multimodal imaging at the initial visit. Examinations included best-corrected visual acuity (BCVA) measurement (decimal visual acuity), intraocular pressure assessment, refraction (RM8900, Topcon, Japan), axial length measurement (OA-2000, Tomey, Japan), and slit-lamp biomicroscopy. Multimodal imaging comprised spectral-domain optical coherence tomography (SD-OCT; Spectralis, Heidelberg Engineering, Germany), optical coherence tomography angiography (OCTA; PLEX Elite 9000, Carl Zeiss Meditec, Germany), fluorescein angiography (FA) and indocyanine green angiography (ICGA; Spectralis HRA and Optos California), color fundus photography (DRI OCT Triton, Topcon, Japan), and fundus autofluorescence (FAF; Spectralis HRA, Heidelberg Engineering). Furthermore, we performed VVA evaluations via ultrawidefield scanning laser fundus imaging-guided swept-source OCT (Optos Silverstone).

VVA evaluation

This study focused on evaluating the superior and inferior VVA located in the temporal quadrants of the fundus. The VVA evaluations were conducted as follows using Optos Silverstone (Fig. 3): (1) Guided by ultrawidefield scanning laser ophthalmoscope images, we performed 3–5 OCT volume scans (6 mm × 6 mm) at strategic locations encompassing and surrounding each VVA (Fig. S2). (2) We acquired a series of choroidal en-face OCT images, each representing a single-pixel depth from the retinal pigment epithelium (RPE) to the sclera (Supplemental video). The RPE was used as the reference boundary, and sequential en-face images were obtained at one-pixel intervals throughout the choroidal depth. To determine the choroidoscleral interface, we analyzed luminance changes along the depth axis at each measurement point. The location of steep luminance increase was identified for every point, and the deepest of these locations was designated as the overall depth. (3) We extracted luminal structures from choroidal en-face images derived from multiple OCT volume scans

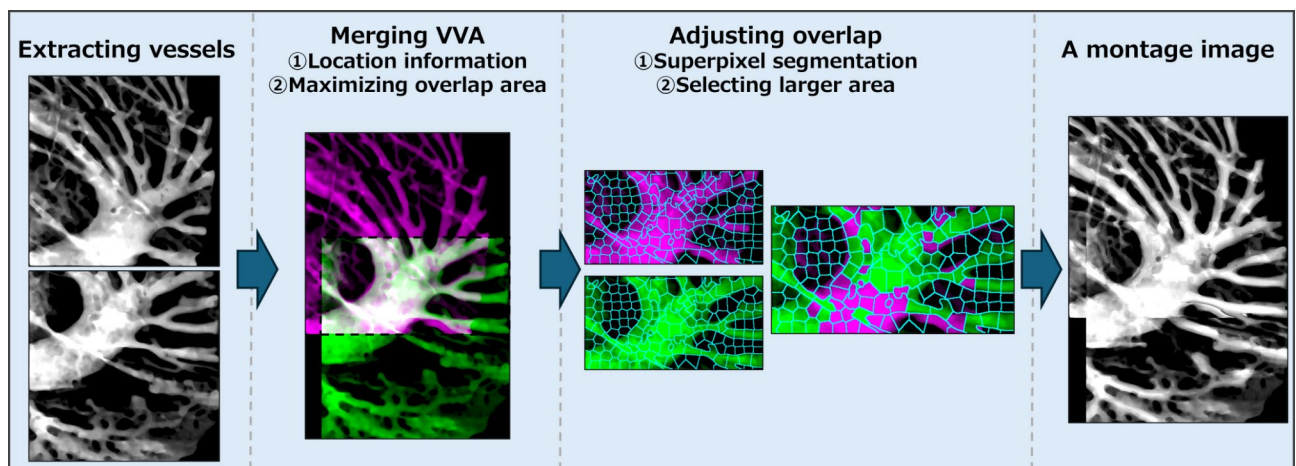


Fig. 3. Process of generating a composite image of the vortex vein ampulla. Multiple en-face optical coherence tomography images acquired in the region of the vortex vein ampullae are aligned on the basis of their positional information. We modified the images to maximize the overlapping areas of the luminal structure and used the superpixel segmentation method to correct for image misalignment.

(Fig. S3). (4) The extracted luminal structures from multiple scans were spatially aligned using the position information recorded during image acquisition. (5) To reduce any misalignments, we implemented an automated algorithm that montaging at maximized the overlap of luminal structures across multiple scans. To mitigate the overestimation of blood vessel volume, we implemented superpixel segmentation using the simple linear iterative clustering (SLIC) method (Fig. 3)⁴⁶. This process was initially applied to the layer with the largest blood vessel area and subsequently extended to all layers. For each corresponding set of superpixels across layers, we selected the one with the largest volume. (6) For vessel skeletonization, we automatically extracted the centerlines of the planar lumina. We subsequently manually corrected any skeletons that deviated significantly from the apparent lumen orientation. We then implemented an automated algorithm to adjust the centerline of the lumen structure along the depth axis. This process estimates the true center of the lumen throughout its depth, allowing us to obtain accurate skeletal information on the vessel structure. (7) On the basis of previously reported methods, we identified the center of each vortex vein ampulla (VVA)²⁰. We then analyzed a defined region surrounding this central point to calculate and quantify VVA morphological parameters.

We expanded the analysis range, starting from an initial diameter of 100 pixels and incrementally increasing it by 100 pixels up to a maximum diameter of 600 pixels. For the interstitial analysis, we focused solely on the areas immediately adjacent to the vessel lumina. We analyzed the following morphological parameters: luminal volume, luminal proportion, total vessel length, and mean vessel diameter.

Statistical analysis

In this study, VVA evaluations were performed twice at different time points for 19 patients and 20 eyes (28 locations total). The reproducibility between these evaluations was assessed using intraclass correlation coefficient (ICC) with a two-way random effects model. A single examiner performed all the examinations, while a single analyst conducted all the analyses. We selected a 400-pixel analysis range for this study based on ICC values. This range demonstrated an ICC > 0.800 for all the items, with the highest ICC for two of the four outcomes and the second highest for the remaining two (Table S5). Participant characteristics and VVA morphological parameters were compared via the Mann-Whitney U test for continuous variables and Fisher's exact test for categorical variables. To compare the VVA morphological parameters across Haller's vessel running patterns, we employed the Kruskal-Wallis test, followed by post hoc Steel-Dwass tests for statistically significant items, adjusting for multiple comparisons.

Associations between the central choroidal thickness (CCT), its related factors (age and axial length)^{47,48}, and VVA morphological parameters were examined using linear regression analysis. Moreover, despite unknown potential confounders influencing VVA morphology, we compared the PSD and control groups via multiple linear regression, adjusting for factors associated with CCT: age, axial length, sex, and Haller vessel running patterns^{14,39,47,48}. P value = 0.05 was set as the statistical cutoff, and we performed all analyses using R software (version 4.3.2).

Meeting presentation

This material was presented at the 39th Annual Meeting of the Japanese Society for Ocular Circulation, Nara, Japan, in 2023.

Data availability

The datasets generated and/or analyzed during the current study are not publicly available because the data release was not included in the research plan and was not communicated to the patients but are available from the corresponding author upon reasonable request.

Received: 11 September 2024; Accepted: 9 December 2024

Published online: 01 April 2025

References

- Pascolini, D. & Mariotti, S. P. Global estimates of visual impairment: 2010. *Br. J. Ophthalmol.* **96**, 614–618 (2012).
- Wong, W. L. et al. Global prevalence of age-related macular degeneration and disease burden projection for 2020 and 2040: a systematic review and meta-analysis. *Lancet Glob Health.* **2**, e106–e116 (2014).
- Pang, C. E. & Freund, K. B. *Pachychoroid Neovascularopathy Retina* **35**, 1–9 (2015).
- Warrow, D. J., Hoang, Q. V. & Freund, K. B. Pachychoroid pigment epitheliopathy. *Retina* **33**, 1659–1672 (2013).
- Miyake, M. et al. Pachychoroid neovascularopathy and age-related macular degeneration. *Sci. Rep.* **5**, 16204 (2015).
- Cheung, C. M. G. et al. *Pachychoroid Dis.* *Eye* **33**, 14–33 (2019).
- Hosoda, Y. et al. Deep phenotype unsupervised machine learning revealed the significance of pachychoroid features in etiology and visual prognosis of age-related macular degeneration. *Sci. Rep.* **10**, 18423 (2020).
- Hata, M. et al. Efficacy of intravitreal injection of aflibercept in neovascular age-related macular degeneration with or without choroidal vascular hyperpermeability. *Invest. Ophthalmol. Vis. Sci.* **55**, 7874–7880 (2014).
- Hata, M. et al. Efficacy of photodynamic therapy for Polypoidal Choroidal Vasculopathy Associated with and without Pachychoroid Phenotypes. *Ophthalmol. Retina.* **3**, 1016–1025 (2019).
- Spaide, R. F. et al. Venous overload choroidopathy: a hypothetical framework for central serous chorioretinopathy and allied disorders. *Prog Retin Eye Res.* **86**, 100973 (2022).
- Imanaga, N. et al. Scleral thickness in Central Serous Chorioretinopathy. *Ophthalmol. Retina.* **5**, 285–291 (2021).
- Imanaga, N. et al. Relationship between Scleral Thickness and Choroidal structure in Central Serous Chorioretinopathy. *Invest. Ophthalmol. Vis. Sci.* **64**, 16 (2023).
- Ishikura, M. et al. Widefield Choroidal thickness of eyes with Central Serous Chorioretinopathy examined by swept-source OCT. *Ophthalmol. Retina.* **6**, 949–956 (2022).
- Funatsu, R. et al. Choroidal morphologic features in central serous chorioretinopathy using ultra-widefield optical coherence tomography. *Graefes Arch. Clin. Exp. Ophthalmol.* **261**, 971–979 (2023).

15. Lee, A., Ra, H. & Baek, J. Choroidal vascular densities of macular disease on ultra-widefield indocyanine green angiography. *Graefes Arch. Clin. Exp. Ophthalmol.* **258**, 1921–1929 (2020).
16. Ryu, G., Moon, C., van Hemert, J. & Sagong, M. Quantitative analysis of choroidal vasculature in polypoidal choroidal vasculopathy using ultra-widefield indocyanine green angiography. *Sci. Rep.* **10**, 18272 (2020).
17. Pang, C. E., Shah, V. P., Sarraf, D. & Freund, K. B. Ultra-widefield imaging with autofluorescence and indocyanine green angiography in central serous chorioretinopathy. *Am. J. Ophthalmol.* **158**, 362–371e2 (2014).
18. Zeng, Q., Yao, Y., Tu, S. & Zhao, M. Quantitative analysis of choroidal vasculature in central serous chorioretinopathy using ultra-widefield swept-source optical coherence tomography angiography. *Sci. Rep.* **12**, 18427 (2022).
19. Matsumoto, H. et al. Pulsation of anastomotic vortex veins in pachychoroid spectrum diseases. *Sci. Rep.* **11**, 14942 (2021).
20. Funatsu, R. et al. Vortex veins in eyes with Pachychoroid Spectrum disorders evaluated by the Adjusted Reverse 3-Dimensional Projection Model. *Ophthalmol. Sci.* **3**, 100320 (2023).
21. Matsumoto, H. et al. Quantitative measures of vortex veins in the posterior Pole in eyes with pachychoroid spectrum diseases. *Sci. Rep.* **10**, 19505 (2020).
22. Kishi, S. et al. Geographic filling delay of the choriocapillaris in the region of dilated asymmetric vortex veins in central serous chorioretinopathy. *PLoS One.* **13**, e0206646 (2018).
23. Kogo, T. et al. Pigment epithelial detachment and leak point locations in Central Serous Chorioretinopathy. *Am. J. Ophthalmol.* **261**, 19–27 (2024).
24. Hayreh, S. S. & Baines, J. A. Occlusion of the vortex veins. An experimental study. *Br. J. Ophthalmol.* **57**, 217–238 (1973).
25. Sodhi, S. K., Golding, J., Trimboli, C. & Choudhry, N. Feasibility of peripheral OCT imaging using a novel integrated SLO ultra-widefield imaging swept-source OCT device. *Int. Ophthalmol.* **41**, 2805–2815 (2021).
26. Imanaga, N. et al. Clinical factors related to Loculation of Fluid in Central Serous Chorioretinopathy. *Am. J. Ophthalmol.* **235**, 197–203 (2022).
27. Sonoda, S. et al. Structural changes of inner and outer choroid in Central Serous Chorioretinopathy determined by Optical Coherence Tomography. *PLoS One.* **11**, e0157190 (2016).
28. Shiihara, H. et al. Quantitative analyses of diameter and running pattern of choroidal vessels in central serous chorioretinopathy by en face images. *Sci. Rep.* **10**, 9591 (2020).
29. Hiroe, T. & Kishi, S. Dilatation of Asymmetric Vortex Vein in Central Serous Chorioretinopathy. *Ophthalmol. Retina.* **2**, 152–161 (2018).
30. Xiao, B., Yan, M., Song, Y. P., Ye, Y. & Huang, Z. Quantitative assessment of choroidal parameters and retinal thickness in central serous chorioretinopathy using ultra-widefield swept-source optical coherence tomography: a cross-sectional study. *BMC Ophthalmol.* **24**, 176 (2024).
31. Maruko, I., Maruko, R., Kawano, T. & Iida, T. Comparisons of choroidal thickness and volume in eyes with central serous chorioretinopathy to that of control eyes determined by ultra-widefield optical coherence tomography. *Graefes Arch. Clin. Exp. Ophthalmol.* <https://doi.org/10.1007/s00417-024-06409-w> (2024).
32. Saito, M., Noda, K., Saito, W. & Ishida, S. Relationship between choroidal blood flow velocity and choroidal thickness in patients with regression of acute central serous chorioretinopathy. *Graefes Arch. Clin. Exp. Ophthalmol.* **256**, 227–229 (2018).
33. Lejoyeux, R. et al. En-face analysis of short posterior ciliary arteries crossing the sclera to choroid using wide-field swept-source optical coherence tomography. *Sci. Rep.* **11**, 8732 (2021).
34. Hayreh, S. S. Segmental nature of the choroidal vasculature. *Br. J. Ophthalmol.* **59**, 631–648 (1975).
35. Bacci, T., Oh, D. J., Singer, M., Sadda, S. & Freund, K. B. Ultra-widefield Indocyanine Green Angiography reveals patterns of choroidal venous insufficiency influencing Pachychoroid Disease. *Invest. Ophthalmol. Vis. Sci.* **63**, 17 (2022).
36. Takahashi, K. & Kishi, S. Remodeling of choroidal venous drainage after vortex vein occlusion following scleral buckling for retinal detachment. *Am. J. Ophthalmol.* **129**, 191–198 (2000).
37. Matsumoto, H. et al. Vortex vein congestion in the monkey eye: a possible animal model of pachychoroid. *PLoS One.* **17**, e0274137 (2022).
38. Terao, N. et al. Short axial length is related to asymmetric vortex veins in central serous chorioretinopathy. *Ophthalmol. Sci.* **1**, 100071 (2021).
39. Funatsu, R. et al. Normal peripheral choroidal thickness measured by widefield optical coherence tomography. *Retina* **43**, 490–497 (2023).
40. Hoshino, J. et al. Variation of vortex veins at the horizontal watershed in normal eyes. *Graefes Arch. Clin. Exp. Ophthalmol.* **259**, 2175–2180 (2021).
41. Shiihara, H. et al. Quantification of vessels of Haller's layer based on en-face optical coherence tomography images. *Retina* **41**, 2148–2156 (2021).
42. Kinoshita, T. et al. Diurnal variations in luminal and stromal areas of choroid in normal eyes. *Br. J. Ophthalmol.* **101**, 360–364 (2017).
43. Funatsu, R. et al. A photodynamic therapy index for Central Serous Chorioretinopathy to Predict Visual Prognosis using pretreatment factors. *Am. J. Ophthalmol.* **253**, 86–95 (2023).
44. van Dijk, E. H. C. et al. Half-dose photodynamic therapy versus high-density Subthreshold Micropulse Laser treatment in patients with Chronic Central Serous Chorioretinopathy: the place Trial. *Ophthalmology* **125**, 1547–1555 (2018).
45. Gomi, F. et al. Initial versus delayed photodynamic therapy in combination with ranibizumab for treatment of polypoidal choroidal vasculopathy: the Fujisan study. *Retina* **35**, 1569–1576 (2015).
46. Achanta, R. et al. SLIC superpixels compared to state-of-the-art Superpixel methods. *IEEE Trans. Pattern Anal. Mach. Intell.* **34**, 2274–2282 (2012).
47. Wei, W. B. et al. Subfoveal choroidal thickness: the Beijing Eye Study. *Ophthalmology* **120**, 175–180 (2013).
48. Mori, Y. et al. Distribution of Choroidal Thickness and Choroidal Vessel Dilation in healthy Japanese individuals: the Nagahama Study. *Ophthalmol. Sci.* **1**, 100033 (2021).

Acknowledgements

During the preparation of this work, the author(s) used Claude 3.5 Sonnet for English proofreading. After using this tool/service, the authors reviewed and edited the content as needed and take full responsibility for the content of the publication.

Author contributions

Author's contributions: RF, HT, SS, MH, YT, HS TS: Conceptualization; RF, NM, HS: Data curation; RF, HT, SS, MH, TS: Writing-Original draft preparation; RF, NM, SS, MH, YT: Visualization, Investigation. HT, SS, HS, YT, TS: Supervision; RF, HT, SS, NM, HS, MH, YT, TS: Writing-Reviewing and Editing.

Funding

This study was supported by JSPS KAKENHI grant numbers 24KJ1842 & 24K12746.

Declarations

Competing interests

Mariko Hirokawa & Yasushi Tanabe are employees of Nikon Corporation. The other authors have no competing interests.

Additional information

Supplementary Information The online version contains supplementary material available at <https://doi.org/10.1038/s41598-024-82731-x>.

Correspondence and requests for materials should be addressed to H.T.

Reprints and permissions information is available at www.nature.com/reprints.

Publisher's note Springer Nature remains neutral with regard to jurisdictional claims in published maps and institutional affiliations.

Open Access This article is licensed under a Creative Commons Attribution-NonCommercial-NoDerivatives 4.0 International License, which permits any non-commercial use, sharing, distribution and reproduction in any medium or format, as long as you give appropriate credit to the original author(s) and the source, provide a link to the Creative Commons licence, and indicate if you modified the licensed material. You do not have permission under this licence to share adapted material derived from this article or parts of it. The images or other third party material in this article are included in the article's Creative Commons licence, unless indicated otherwise in a credit line to the material. If material is not included in the article's Creative Commons licence and your intended use is not permitted by statutory regulation or exceeds the permitted use, you will need to obtain permission directly from the copyright holder. To view a copy of this licence, visit <http://creativecommons.org/licenses/by-nc-nd/4.0/>.

© The Author(s) 2025